International Journal of Computational Intelligence Research
ISSN 0973-1873 Volume 20, Number 1 (2024), pp.21-35

https://dx.doi.org/10.37622/IJCIR/20.1.2024.21-35

Lung Disease Recognition Using Ensemble Deep Net Model for Disease Identification and Classification

[1]Dr. Aziz Makandar and [2]Miss. Nayan Jadhav*

[1]Professor and [2]Research Scholar
Department of Computer Science, Karnataka State Akkamahadevi women's University, Vijayapura, Karnataka, India.
Corresponding author: (*E-mail: jadhavnayan321@gmail.com****)***

Abstract

This research introduces a groundbreaking approach for identification of lung diseases, with a focus on improving patient outcomes and easing the burden on healthcare systems. The primary goal is to enable precise prediction of lung diseases at an early stage. The proposed hybrid model, CNN-GRU-LSTM, is employed for analyzing sequential lung images. An Ensemble Deep Net model is introduced, incorporating CNNs, VGG-based neural networks, and Caps networks. A key innovation is the Spatio Temporal Deep (STD) feature, which captures global and local contextual information across multiple frames. The evaluation of the hybrid model on a diverse dataset demonstrates its effectiveness in identifying subtle patterns indicative of early-stage lung diseases. The Ensemble Deep Net model achieves exceptional accuracy in lesion detection within the complex and variable landscape of lung nodules. The Ensemble Deep Net is leveraged to achieve a remarkable 100% accuracy in classifying diverse lung diseases. This research marks a significant advancement in pulmonary healthcare by providing a valuable tool for early diagnosis and intervention in lung diseases. Also, it holds great promise for enhancing preventive strategies in pulmonary medicine offering a revolutionary path for improving patient care.

Keywords: *Convolutional Neural Network (CNN); Gated Recurrent Unit (GRU); Long Short-Term Memory network (LSTM); Visual Geometry Group-based neural network (VGG); Chronic Obstructive Pulmonary Disease; Spatio Temporal Deep.*

INTRODUCTION

In the wake of evolving environmental conditions, rising temperatures, lifestyle shifts, and various contributing factors, the impact of illnesses on global health is undergoing a swift and alarming escalation. In this context, advanced technologies and comprehensive medical analyses become paramount in addressing the burgeoning global health challenges and safeguarding human well-being [1]. Especially in developing and low-income countries, where billions grapple with poverty and air pollution, the risk of lung disorders is notably high. Since late December 2019, the novel coronavirus infection (COVID-19) has been inflicting severe damage on the lungs, leading to respiratory complications. Furthermore, respiratory infections, categorized as a form of lung disease, can be exacerbated by the virus responsible for COVID-19 or by other viral or bacterial infections [2].

Pneumonia, pneumothorax, and Tuberculosis (TB) stand out as leading causes of global fatalities related to lung diseases. Complete or total lung collapse can occur as a result of the illness mesothelioma [3]. Intense activity like climbing mountains, travelling, or diving for pleasure may result in a collapse of the lungs. These vigorous actions might result in significant variations in pressure in the air. This condition symptoms frequently including fatigue, skin that is blue and difficulty from breathing, wild respiration, a dry, whooping pain in the chest and a wheeze. A lung infection brought on by an airborne bacterium called tuberculosis. TB symptoms include a coughing fit that persists for three weeks straight, a lack of hunger that results in unintentional loss of weight, chills, a fever, and night sweats [4].

Thus, early detection and evaluation can considerably lessen risk that lung illnesses pose to life to improve the standard of living for those who are afflicted. Imagery procedures are incredibly dependable tools for diagnosis in modern medicine picture methods that may aid specialists in the diagnosis of several ailments. They are diagnostic gadgets that enable medical professionals in order to see inside organs of human body deprived of having to cut [5].

An experienced physician now conducts lung disease detection using an examination of Chest X-Ray images due to its convenience and minimum demand for an explanation of the thoracic condition in brief. It is especially ideal for subsequent examinations since sickness changes may be identified more quickly and easily. But because of the complicated anatomical framework of the chest, it is a common human mistake for a CXR imaging to be misinterpreted. In an effort to avoid misunderstanding and help radiologist generate more precise diagnoses that can replace clinical judgements, radiologist use Computer-Aided Diagnostic Systems (CAD). Numerous methods have made considerable use of the Chest X-Ray image to enhance the efficacy and accuracy of CADs' diagnosing capabilities [6].

Key contribution

Ensemble Model Integration (EMI): The utilization of an ensemble model incorporating CNN, LSTM, VGG, and GRU architectures is a novel approach. This

integration capitalizes on the unique strengths of each component, resulting in a synergistic effect that enhances overall performance and robustness in detecting various lung diseases.

Comprehensive Feature Analysis (CFA): By considering multiple features, the model conducts a thorough analysis that captures a diverse range of characteristics relevant to the development of lung diseases. This comprehensive feature exploration significantly improves the model's capacity to accurately identify and classify different types of lung conditions, addressing the complexity and variability inherent in such diseases.

Spatio Temporal Deep (STD) Feature: The introduction of the STD feature represents a novel contribution. This feature takes into account both global and local contextual information across sequential images, allowing the model to capture the dynamic changes and progression of lung nodules over time. This consideration of spatio temporal dynamics enhances the model's capability for early detection and accurate prediction of lung diseases, offering a valuable advancement in the field of medical image analysis.

2. LITERATURE REVIEW

Early detection of cancer, such as adenocarcinoma of the lungs (LA), significantly improves the chances of successful therapy. To achieve optimal early diagnosis, researchers utilize machine learning to analyze patterns in blood biochemistry. Using sparse regression-based machine learning, researchers identify early stages of LA, developing a set of seven diagnostic indicators. However, challenges include material complexity and metabolite quantity affecting mass spectrometry detection, requiring significant prior treatment techniques for compound extraction and segregation from complex bio-mixtures [7].

Utilizing enhanced OCLR machine learning, researchers analyze transcriptomes and regulatory sets of non-transformed primordial stem cell features, including their progeny. Results indicate that the dedifferentiated carcinogenic phenotype may be more prevalent in distant tumors. When applied to single-cell data, the stemness scores sequence reveals intra-tumor genetic variation. However, some findings raise questions about the therapy's efficacy, particularly in relation to specific HNSC genes [8]. Artificial intelligence algorithms for pathological identification that were diagnosed with lung lesions verified on massive amounts tests have yet to be seen, despite recent evidence that AI deep learning models are useful in a variety of medical fields. This research built a Convolution Neural Network (CNN) centered on EfcientNet-B3 architecture, employing transfer learning and weakly-supervised learning for identifying cancer in WSIs. The creation and validation of algorithms like theirs lessen the workload for pathologists [9].

This study explores the potential of blood-borne microRNA (miRNA) biomarkers as circulatory markers for identifying lung cancer in a larger cohort of symptomatic patients and healthy controls. The results, derived from diverse scenarios and group studies, aim for thorough validation. However, the study emphasizes that circulatory

biomarker testing should not replace established methods like neuroimaging, sputum cytology, or biopsy testing [10].

This study explores the role of tumor stem cells in the progression of lung squamous cell carcinoma (LSCC), investigating the regulatory processes associated with LSCC stem cells. Employing weighted gene co-expression network analysis (WGCNA), the study identified significant genes linked to LSCC mRNAsi. Five key genes regulating LSCC mRNAsi were highlighted, showing enhanced activity in cancerous tumors compared to normal tissues. These genes have implications for targeted treatment to mitigate the therapeutic characteristics of LSCC by inhibiting cancer cell stem cell traits. While promising, further research is needed to validate these findings, as they rely on retrospective data [11].

3. PROBLEM STATEMENT

The global prevalence of lung diseases highlights the urgency of early detection for effective public health management. However, the diverse nature of lung nodules and intricate surrounding structures poses a challenge for existing machine learning (ML) and image processing models. Despite previous developments, these models often struggle to address the wide spectrum of lung nodules and the complexities of surrounding tissues. Recognizing the limitations of basic convolutional neural network (CNN) models in handling rotated, slanted, or aberrant image orientations common in medical imaging, the planned ensemble approach seeks to overcome this challenge.

4. METHODS AND MATERIALS

This dataset forms the foundation for subsequent steps in the development of an Ensemble Deep Net model for accurate lung disease prediction.

Step 1: Dataset Acquisition: Acquire a diverse lung disease image dataset, ensuring representation of various conditions to facilitate a thorough analysis. The dataset should cover instances of pneumonia, asthma, TB, fibrosis, COPD, and other relevant categories.

Step 2: Pre-processing Steps: Prepare the image dataset for training and testing by implementing pre-processing steps. This involves resizing images, normalizing pixel values, and addressing any noise or artifacts present in the data. Ensuring uniformity in image characteristics enhances the model's ability to extract meaningful features.

Step 3: Feature Extraction: Perform feature extraction on the pre-processed lung disease images. This includes extracting both handcrafted features and deep features. The incorporation of the Spatio Temporal Deep (STD) feature allows for the capture of global and local circumstances over frames, harnessing the advantages of deep features for accurate prediction of lung diseases.

Step 4: Ensemble Deep Net Model Construction: Construct the Ensemble Deep Net model, comprising multiple deep learning architectures—CNN, LSTM, VGG, and

GRU. CNN and VGG are adept at image analysis tasks, while LSTM and GRU capture temporal dynamics in sequential data. Train each individual architecture separately, fine-tuning them to extract the most relevant features for the specific task of lung disease prediction.

Step 5: Ensemble Model Integration: Integrate the predictions of individual deep learning architectures using an ensemble learning approach. This can involve averaging output probabilities or employing advanced techniques like stacking or boosting. This integration aims to capitalize on the strengths of each architecture, enhancing the overall predictive performance.

Step 6: Results Analysis: Analyze the outcomes of the Ensemble Deep Net model, interpreting its accuracy rate and performance across various lung disease classes such as "Mass," "Nodule," "Pneumothorax," "Consolidation," "Pleural Thickening," and "Cardiomegaly." Evaluate the model's ability to detect and classify lung diseases accurately.

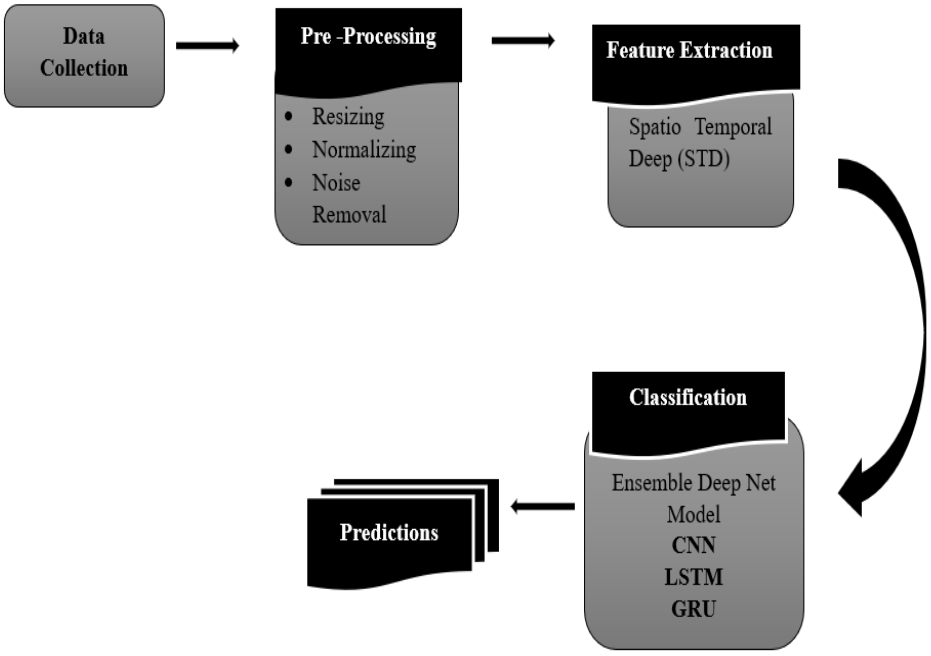

Figure 1. Block diagram of lung diseases prediction

Figure 1 shows the visual representation of the lung diseases prediction workflow, illustrating the sequential steps from dataset acquisition to ensemble model integration.

4.1. Data collection

The dataset includes vital details such as age, medical data, sex, and X-ray images, providing a holistic foundation for model development. Table 1 below shows the dataset for lung disease detection, encompassing both chest X-ray and CT scan images.

Table 1. Dataset description report

Diseases	Dataset type	Name of classes	Sub class images		Total Instances
			Train	Test	
Lung's disease	CT scan and Chest X-ray images	1. Mass	280	150	
		2. Nodule	280	150	
		3. Consolidation	280	150	
		4. Cardiomegaly	280	150	
		5. Pneumothorax	280	150	
		6. Pleural thickening	280	150	2580

4.2. Data pre-processing

Pre-processing techniques play a crucial role in preparing input images for effective model training. This involves resizing images, normalizing pixel values, and addressing noise or artifacts present in the data. The quality and informativeness of the dataset are improved by using techniques including channel segregation, cropping. Cropping is used to remove external parts of images, improving framing, altering angles, and emphasizing specific subjects. Resizing is applied to alter the physical size of images.

4.3. Spatiotemporal CNN Feature Extraction

Feature extraction includes extracting both handcrafted features and deep features. The incorporation of the Spatio Temporal Deep (STD) feature allows for the capture of global and local circumstances over frames, harnessing the advantages of deep features for accurate prediction of lung diseases.

Local feature extraction: This method involves obtaining region-based features by feeding divided regions, or super pixels, into a region-based Convolutional Neural Network (CNN) at each frame. Instead of a simple average across frames, which could lead to reduced accuracy due to pixel instability from lossy compression over time, the researchers employ a Gaussian distribution centered at neighboring images' regions. The local feature $U\ P$ (P , □) of an area i at frame □ is extracted by,

$$U_P(i,h) = \frac{1}{\psi}\sum_{h'}^{h+\frac{k}{2}} g(h'\,|h,\sigma^2)u(i,h') \quad (1)$$

Where $u(i,h')$ is area i's zone-based feature at frameworkh', and k = 16 indicates how many frames are involved in the process. $g(h'|h,\sigma^2)$ Is a Gaussian distribution having a mean of h and an SD. $|\sigma = 2)$representing the temporal weighted dispersion ψ the adjusting factor?

Global feature extraction: The methodology forming a chronological segment, into a block-based Convolutional Neural Network (CNN) to compute its global characteristics. This approach ensures the consideration of temporal stability in deriving the global characteristic [13]. The researchers adopt an efficient approach by inputting each input unit into the pre-trained C3D model only once, followed by assigning the exact same value for the extracted global feature (U_S (h)) to every block's region. Subsequently combine both the global and local characteristics of each region in every

image to create the STD feature $U\,P\ (i\ ,\ \square)$ of the location i at image □, which has a height of 4096x2 is expressed in Eqn. (2)

$$U(i,h) = U_P(i,h) \oplus U_S(h) \qquad (2)$$

4.4. Ensemble-CNN-GRU-LSTM model for classification

The utilization of deep ensemble learning models brings forth improved generalization by harnessing the definitive assets of both DL and ensemble learning. In the ensemble model (CNN, LSTM, VGG, and GRU), CNN and VGG are proficient at image analysis tasks, while LSTM and GRU capture temporal dynamics in sequential data. This approach highlights the power of collaborative learning and the enhanced predictive capabilities achieved through the amalgamation of deep and ensemble learning techniques.

4.4.1. VGG19 and Deep CNN with multi-pooling layer

VGG-19 comprises of 3 fully connected layers and 16 convolutional layers. A notable feature is the use of 3x3 pixel filters in convolutional layers. In total, VGG-19 comprises approximately 138 million calculation parameters, showcasing its complexity and depth in neural architecture. This model is recognized for its effectiveness in image recognition tasks, particularly due to its meticulous layer design and strategic use of convolutional filters [14]. The training of VGG-16 utilized the ImageNet following the max-pooling layers, three fully connected layers are incorporated, and the design culminates with a SoftMax classifier as the final layer. The application of ReLU activation functions across all hidden layers significantly enhances the overall efficiency of the VGG-16 network in tasks related to image classification [15].

4.4.2. Gated Recurrent Unit (GRU)

The GRU network presents a refined version of the Long Short-Term Memory (LSTM) cell, maintaining its efficacy while simplifying its structure. Each GRU cell incorporates two essential gates: the reset gate (t) and the update gate (t). The reset gate, akin to LSTM, governs the balance between retaining old information and incorporating new information, allowing for the capture of periodic correlations in the data. The update gate, on the other hand, determines the extent to which past knowledge is "forgotten," facilitating effective memorization of input data $x\,t$ of varying lengths in Figure 2 [16].

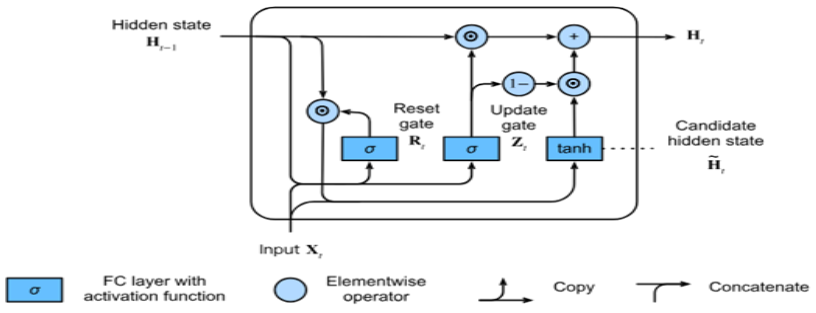

Figure 2. Architecture of GRU model

GRU's fundamental steps are as follows:

Initially, the most recent input x_t interacts with the hidden condition set by the preceding cellh_{t-1}, along with the output from the reset gate j_t and the update gate v_t at the current time step. The outputs of these two gates are articulated as per Equations (3) and (4):

$$j_t = \sigma\left(w^j[h_{t-1}, x_t] + b^j\right) \quad (3)$$

$$v_t = \sigma(w^v[h_{t-1}, x_t] + b^z) \quad (4)$$

Where w^j and $w^v$are the proper weight coefficient matrices, $b^j$and $b^z$are bias the vectors, and $\sigma()$is sigmoid purpose.

The concealed state $\tilde{h}_t$ stated as follows in Eqn. (5):

$$\tilde{h}_t = tanh(\, w^h[(h_{t-1} * j_t), x_t] + b^h) \quad (5)$$

Here, the hyperbolic tangent function (tanh) is applied, wherew^h represents the pertinent matrix of weight coefficients for the hidden layer, b^h is the associated bias vector, and * denotes the matrix dot multiplication between corresponding pairs. To conclude, the current hidden state h_t output is determined by linearly combining the current candidate hidden state $\bar{h}_t$ and the preceding hidden state h_{t-1}, with a total of weighted coefficients as expressed in Equation (6).

$$h_t = (1 - v_t) * \bar{h}_t + v_t * h_{t-1} \quad (6)$$

The disparity among the anticipated real figures for a certain data example determines what actually happened. Underneath a network's hidden layers, a weighted parameter alters input data. Nodes, sometimes referred to as cells, make up a neural network. A collection of inputs, a weight, and a bias value are present for every node.

4.4.3. Long Short-Term Memory Networks (LSTM)

LSTMs apart is their recurrent nature, featuring gates that facilitate precise data flow and effectively alleviate short-term memory limitations. In the LSTM structure, the evolution of long-term memory is denoted as the "cell state," and this progression is regulated by three key gates: input, forget, and output. These gates act as intelligent filters, each assigned a specific role in the management and processing of information. The innovative architecture of LSTMs renders them highly efficient in tasks demanding an understanding of temporal dependencies, providing state-of-the-art solutions to prediction problems. Refer to Figure 3 for a visualization of the LSTM model architecture.

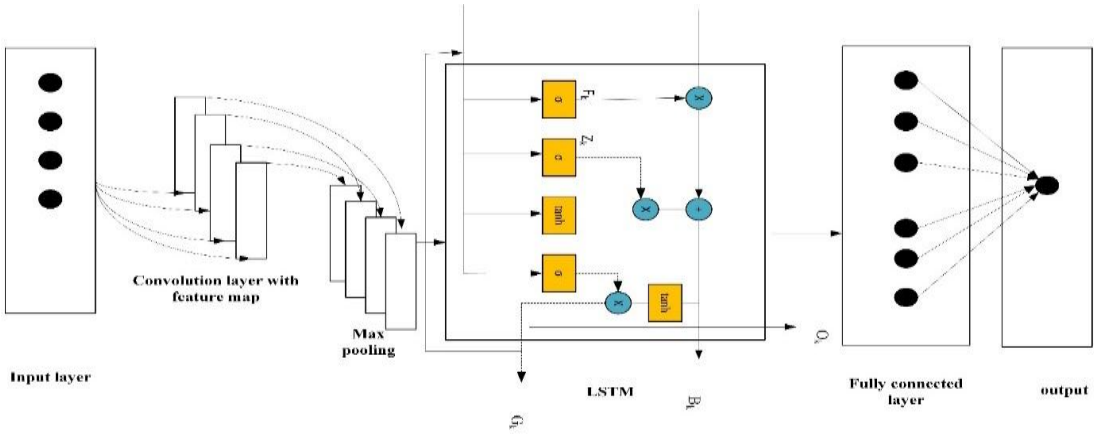

Figure 3. LSTM Framework

LSTM's fundamental steps are as follows:

Input Gate: Tasked with making decisions based on the preceding hidden state and recently introduced input data, this gate is responsible for selecting the new data to be incorporated into the LSTM cell state. The fundamental operating principles of the LSTM input gate, as outlined in Equations (7) to (9), elaborate on the mechanism by which it identifies and integrates relevant information into the cell state while filtering out less significant data.

$$i_{0_t} = \sigma(W_i.[h_{t-1}, X_t] + b_i) \quad (7)$$

$$\tilde{C}_{0_t} = \tanh(W_i.[h_{t-1}, X_t] + b_i) \quad (8)$$

$$C_{0_t} = f_t C_{t-1} + i_t \tilde{C}_{0_t} \quad (9)$$

$Where, W_i\ stands\ for\ weight\ matrix.$

$b_i\ =\ biased\ input\ gates$

$C_{0_t}\ =\ information\ from\ memory$

$\tilde{C}_{0_t}\ =\ production\ of\ tanh$

Forget Gate: Operating based on the previously hidden state and newly introduced input data, this gate plays a crucial role in deciding the relevance of specific bits within the cell state. The principles governing the operation of the forget gate are succinctly outlined in Equation (10), encapsulating the process by which it identifies and retains essential information while discarding less pertinent bits.

$$f_{0_t} = \sigma\left(W_f.[h_{t-1}, X_t] + b_f\right) \quad (10)$$

Where, W_f displays the weighted matrix.

b_f = offsets

σ = sigmoid curve

Output Gate: Based on the most recent cellular state, the priority hidden state, and the latest input data, the output gate is responsible for determining the updated hidden state, as expressed in Equation (11). The resulting gate principle outlined in Equation (12) can be illustrated through the following equation:

$$O_{0_t} = \sigma(W_0.[h_{t-1}, X_t] + b_0) \quad (11)$$

$$h_t = O_{0_t} \tanh(C_{0_t}) \quad (12)$$

Where, W_0 represent the output gate's balanced vectors.

b_0=Bias of LSTM

The integration of networks offers a potent blend of sequential modelling and image processing capability.

4.4.4. Hybrid model CNN-LSTM-GRU

CNN-GRU: The integration of CNN with GRU brings together the ability of CNNs to extract spatial features from images and GRU's proficiency in capturing temporal dependencies. This synergy is particularly advantageous for tasks involving both spatial and temporal aspects, such as video analysis. The CNN processes the spatial features of the input images, and the GRU captures sequential patterns over time. This combination is highly effective in tasks where understanding both visual content and temporal relationships is crucial.

CNN-LSTM: Similar to CNN-GRU, the coupling of CNN with LSTM leverages the strengths of CNNs in image feature extraction and LSTM's capability to capture long-range dependencies in sequential data. CNN focuses on spatial features, extracting meaningful representations from images, while LSTM handles sequential data, enabling the model to comprehend and remember intricate patterns over extended sequences.

In work, both CNN-GRU and CNN-LSTM architectures offer a sophisticated approach to tasks demanding a holistic understanding of both spatial and temporal aspects in data, showcasing the synergy between convolutional and recurrent neural networks. The choice between GRU and LSTM depends on the specific requirements of the task, with both configurations demonstrating efficacy in various applications.

RESULT AND DISCUSSION

The results encompass an analysis of the proposed algorithm's performance in predicting lung diseases. This summary encapsulates the experimental methodology and the subsequent evaluation of the proposed technique, emphasizing its application in the domain of lung disease prediction.

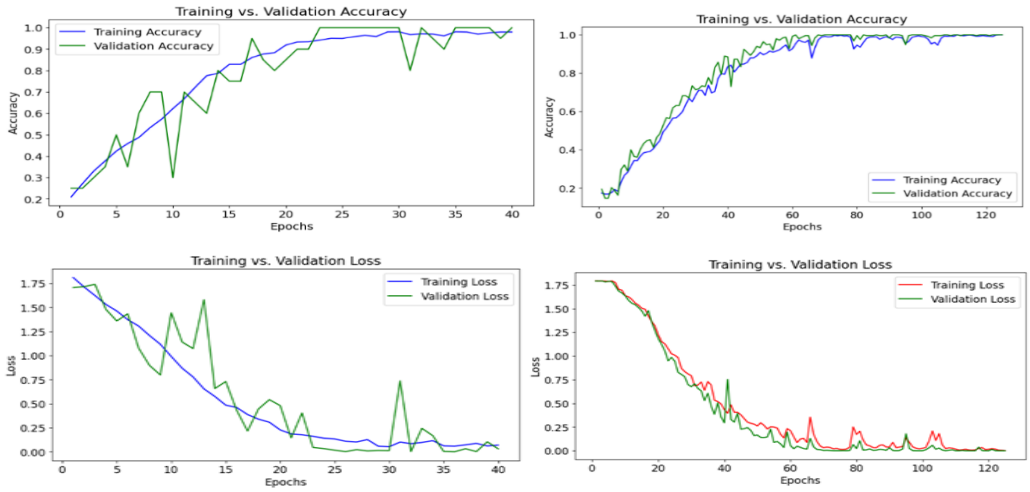

A. CNN-GRU **B. CNN-LSTM**

Figure 4. Accuracy and loss in training time and validation time

Figure 4 shows the training and validation accuracy and loss under various epochs for two model combinations A) CNN-GRU and B) CNN- LSTM.

Table 2 provides a detailed overview of the performance metrics derived from a classification report for the A) CNN- GRU B) CNN- LSTM models.

Table 2. CNN-GRU and CNN-LSTM categorization statistics for the framework

	Precision	**Recall**	**F1-score**	**Support**
Cardiomegaly	0.99	1.00	1.00	150
Consolidation	1.00	1.00	1.00	150
Mass	0.99	1.00	1.00	150
Nodule	1.00	0.99	1.00	150
Pleural thickening	1.00	1.00	1.00	151
Pneumothorax	1.00	0.99	1.00	150
Accuracy			1.00	901
Macro avg	1.00	1.00	1.00	901
Weighted avg	1.00	1.00	1.00	901

	Precision	**Recall**	**F1-score**	**Support**
Cardiomegaly	1.00	1.00	1.00	140
Consolidation	1.00	1.00	1.00	140
Mass	1.00	1.00	1.00	140
Nodule	1.00	1.00	1.00	140
Pleural thickening	1.00	1.00	1.00	140
Pneumothorax	1.00	1.00	1.00	140
Accuracy			1.00	840
Macro avg	1.00	1.00	1.00	840
Weighted avg	1.00	1.00	1.00	840

A. CNN-GRU **B. CNN-LSTM**

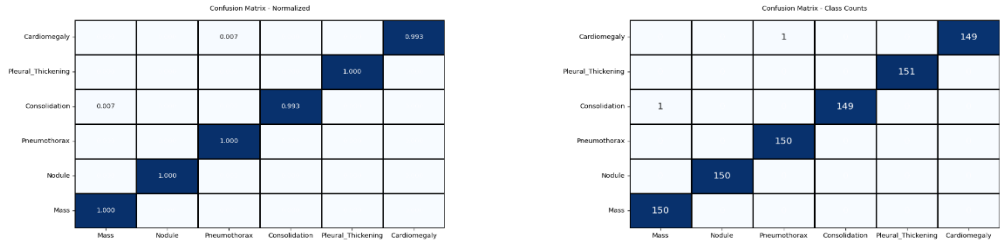

(a) Normalized **(b) Class count**

A.CNN-GRU

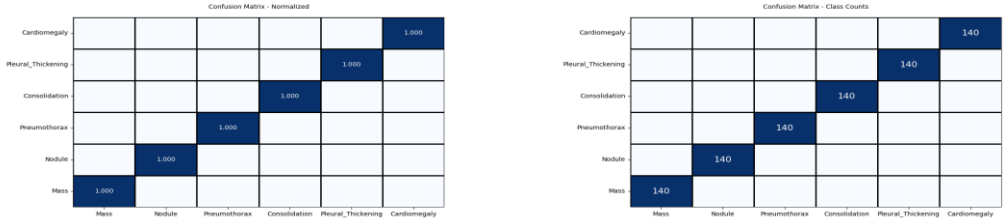

(a) Normalized **(b) Class count**

B. CNN-LSTM

Figure 5. Confusion metrics for model CNN-GRU and CNN-LSTM with respective normalized and class count

Figure 5 shows confusion matrix values of two models A) CNN-GRU and B) CNN-LSTM respectively. It gives a clear image of how many forecasts were accurate and inaccurate for each class, enabling a direct comparison of performance between classes.

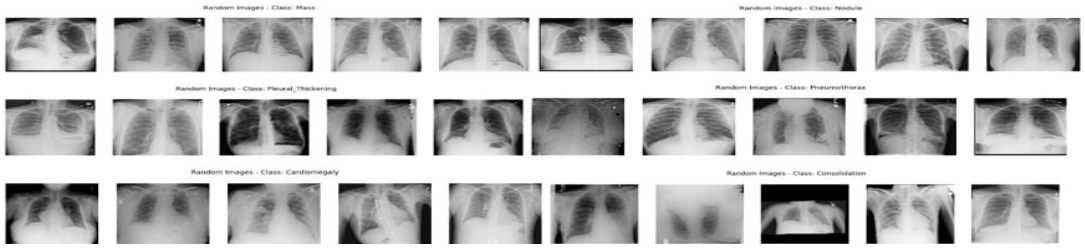

Figure 6. Classification images

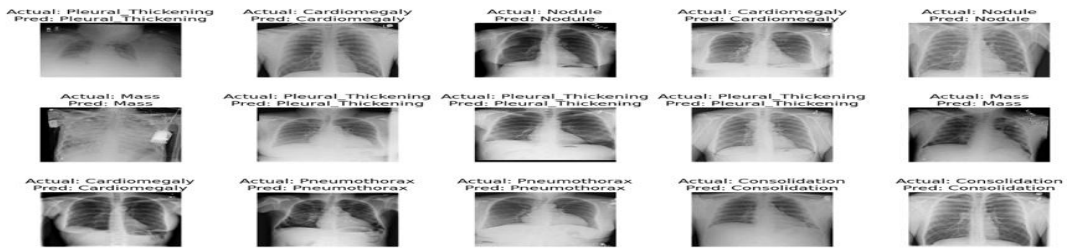

Figure 7. Predicated results on dataset

Figure 6 shows the representation of classification images with respective classes. Figure 7 shows the overall predicated results on classification of the given dataset with respective models a) CNN-GRU b) CNN-LSTM

Table 3 illustrates the comparisons of the acquired accurateness with the proposed methods and other classifications.

Table 3. Comparison table

	Class	Precision	Recall	F1-score
Proposed Model (CNN-GRU)	**Cardiomegaly**	**0.99**	**1.00**	**1.00**
	Consolidation	**1.00**	**1.00**	**1.00**
	Mass	**0.99**	**1.00**	**1.00**
	Nodule	**1.00**	**0.99**	**1.00**
	Pleural Thickening	**1.00**	**1.00**	**1.00**
	Pneumothorax	**1.00**	**0.99**	**1.00**
(CNN-LSTM)	**Cardiomegaly**	**1.00**	**1.00**	**1.00**
	Consolidation	**1.00**	**1.00**	**1.00**
	Mass	**1.00**	**1.00**	**1.00**
	Nodule	**1.00**	**1.00**	**1.00**
	Pleural Thickening	**1.00**	**1.00**	**1.00**
	Pneumothorax	**1.00**	**1.00**	**1.00**
VGG19	Cardiomegaly	81.6	83.2	82.1
	Consolidation	86.8	80.4	84.3
	Mass	84.2	88.7	89.2
	Nodule	81.8	87.4	85.5
	Pleural Thickening	84.8	83.4	83.7
	Pneumothorax	82.9	89.2	86.2
Random Forest	Cardiomegaly	92.3	94.2	91.3
	Consolidation	89.1	90.4	88.2
	Mass	91.4	89.2	90.1
	Nodule	78.4	76.2	76.3
	Pleural Thickening	82.8	85.9	81.6
	Pneumothorax	81.9	82.7	84.5
CNN	Cardiomegaly	86.3	89.5	84.4
	Consolidation	89.1	91.2	90.3
	Mass	83.8	81.2	80.2
	Nodule	85.1	89.9	84.6
	Pleural Thickening	83.5	84.1	86.2
	Pneumothorax	82.3	84.2	86.2

CONCLUSION

The research introduces a powerful Ensemble Deep Net model that combines the strengths of CNN, LSTM, GRU, and VGG networks to elevate the accuracy and robustness of lung disease prediction. An Ensemble Deep Net model is introduced, incorporating CNNs, VGG-based neural networks, and Caps networks. A key innovation is the Spatio Temporal Deep (STD) feature, which captures global and local contextual information across multiple frames. The evaluation of the hybrid model on a diverse dataset demonstrates its effectiveness in identifying subtle patterns indicative of early-stage lung diseases. The Ensemble Deep Net model achieves exceptional

accuracy in lesion detection within the complex and variable landscape of lung nodules. The incorporation of the innovative Spatio Temporal Deep feature enables the model to capture both global and local contextual information across multiple frames, significantly enhancing its capacity to comprehend the temporal dynamics inherent in lung diseases. This improvement addresses limitations observed in basic CNN models, particularly in handling variations in image orientations, leading to greater robustness and adaptability in diverse imaging scenarios. Extensive experimental evaluations substantiate the model's effectiveness, showcasing an impressive 100% accuracy rate in classifying various clinically significant lung conditions marking a substantial contribution to the field of lung disease detection.

REFERENCE

[1] S. Bharati, P. Podder, R. Mondal, A. Mahmood, and Md. Raihan-Al-Masud, "Comparative Performance Analysis of Different Classification Algorithm for the Purpose of Prediction of Lung Cancer," in Intelligent Systems Design and Applications, vol. 2, p. 6-8, 2020.

[2] M. R. H. Mondal, S. Bharati, P. Podder, and P. Podder, "Data analytics for novel coronavirus disease," Inform. Med. Unlocked, vol. 20, p. 100374, Jan. 2020, doi: 10.1016/j.imu.2020.100374.

[3] N.-C. Huan, C. Sidhu, and R. Thomas, "Pneumothorax: classification and etiology," Clin. Chest Med., vol. 42, no. 4, pp. 711–727, 2021.

[4] A. Dumas et al., "The host microbiota contributes to early protection against lung colonization by Mycobacterium tuberculosis," Front. Immunol. vol. 9, p. 2656, 2018.

[5] S. T. H. Kieu, A. Bade, M. H. A. Hijazi, and H. Kolivand, "A Survey of Deep Learning for Lung Disease Detection on Medical Images: State-of-the-Art, Taxonomy, Issues and Future Directions," J. Imaging, vol. 6, no. 12, Art. No. 12, Dec. 2020, doi: 10.3390/jimaging6120131.

[6] S. Kim, B. Rim, S. Choi, A. Lee, S. Min, and M. Hong, "Deep Learning in Multi-Class Lung Diseases' Classification on Chest X-ray Images," Diagnostics, vol. 12, no. 4, Art. No. 4, Apr. 2022, doi: 10.3390/diagnostics12040915.

[7] L. Huang et al., "Machine learning of serum metabolic patterns encodes early-stage lung adenocarcinoma," Nat. Commun., vol. 11, no. 1, pp. 1–11, 2020, doi: https://doi.org/10.1038/s41467-020-17347-6.

[8] T. M. Malta et al., "Machine Learning Identifies Stemness Features Associated with Oncogenic Dedifferentiation," Cell, vol. 173, no. 2, pp. 338-354.e15, Apr. 2018, doi: 10.1016/j.cell.2018.03.034.

[9] X. Ren et al., "Weakly supervised label propagation algorithm classifies lung cancer imaging subtypes," Sci. Rep., vol. 13, no. 1, Art. No. 1, Mar. 2023, doi: 10.1038/s41598-023-32301-4.

[10] T. Fehlmann et al., "Evaluating the Use of Circulating MicroRNA Profiles for Lung Cancer Detection in Symptomatic Patients," JAMA Oncol., vol. 6, no. 5, pp. 714–723, May 2020, doi: 10.1001/jamaoncol.2020.0001.

[11] S. Qin, X. Long, Q. Zhao, and W. Zhao, "Co-expression network analysis identified genes associated with cancer stem cell characteristics in lung squamous cell carcinoma," Cancer Invest., vol. 38, no. 1, pp. 13–22, 2020, doi: https://doi.org/10.1080/07357907.2019.1697281.

[12] T.-N. Le and A. Sugimoto, "Video Salient Object Detection Using Spatiotemporal Deep Features," IEEE Trans. Image Process., vol. 27, no. 10, pp. 5002–5015, Oct. 2018, doi: 10.1109/TIP.2018.2849860.

[13] A. El Kaid, K. Baïna, and J. Baïna, "Reduce False Positive Alerts for Elderly Person Fall Video-Detection Algorithm by convolutional neural network model," Procedia Comput. Sci., vol. 148, pp. 2–11, 2019, doi: 10.1016/j.procs.2019.01.004.

[14] D. Theckedath and R. R. Sedamkar, "Detecting Affect States Using VGG16, ResNet50 and SE-ResNet50 Networks," SN Comput. Sci., vol. 1, no. 2, p. 79, Mar. 2020, doi: 10.1007/s42979-020-0114-9.

[15] H. Niu, K. Xu, and C. Liu, "A decomposition-ensemble model with regrouping method and attention-based gated recurrent unit network for energy price prediction," Energy, vol. 231, p. 120941, Sep. 2021, doi: 10.1016/j.energy.2021.120941.